IEEE Access
Multidisciplinary ⋮ Rapid Review ⋮ Open Access Journal

Received 28 May 2026, accepted 21 June 2026, date of publication 6 July 2026, date of current version 22 July 2026.

Digital Object Identifier 10.1109/ACCESS.2026.3710402

RESEARCH ARTICLE

Inverse Probabilistic Security-Constrained Optimal Power Flow for Reliability Parameter Calibration, Transmission Investment, and Standard Setting

FELIPE SEPÚLVEDA [1], DIEGO ALVARADO [2], FELIPE CORDERA [3], EDUARDO ESPERGUEL [4], GORAN STRBAC [5], (Fellow, IEEE), AND RODRIGO MORENO [6], (Member, IEEE)

[1] Department of Industrial Engineering, University of Chile, Santiago 8370456, Chile
[2] Department of Electrical Engineering, University of Chile, Santiago 8320000, Chile
[3] Operation Research Center, Massachusetts Institute of Technology, Cambridge, MA 02139, USA
[4] National Energy Commission, Santiago 8340518, Chile
[5] Department of Electrical and Electronic Engineering, Imperial College London, SW7 2AZ London, U.K.
[6] Faculty of Engineering and Sciences and the Business School, Universidad Adolfo Ibáñez, Santiago 7941169, Chile

Corresponding author: Felipe Sepúlveda (felisepulveda@ug.uchile.cl)

This work was supported in part by Agencia Nacional de Investigación y Desarrollo (ANID), Chile, under Grant FONDECYT 1231924 and Grant FOVI 250225.

ABSTRACT Network reliability standards should ideally be informed by quantitative probabilistic models that quantify the costs and benefits associated with different levels of supply-quality improvement. However, these probabilistic models, such as those used to determine transmission network investments, require component-level outage and repair rates that are frequently missing or incomplete. To address this limitation, this paper proposes a two-part framework that first infers these missing input parameters and then delivers high-quality assessments of the investment costs required to attain a certain supply-quality level. In the first part, an Inverse Probabilistic Security-Constrained Optimal Power Flow (Inverse PSC-OPF) is developed to infer network-component reliability parameters—specifically outage and repair rates—directly from observed system-level continuity metrics routinely documented by regulatory authorities, namely interruption duration, interruption frequency, and unserved energy. In the second part, these calibrated parameters are integrated into a probabilistic transmission expansion planning model to find economically justifiable supply-quality improvements. We apply the framework to the Chilean transmission system ($\approx$ 2,200 lines/transformers, $\approx$ 2,400 buses), where the resulting optimal investments, together with their costs and benefits across reliability levels, provided insights that informed the formulation of Chile's national transmission reliability standard.

INDEX TERMS Inverse optimization, reliability, reliability parameters, supply continuity metrics.

I. INTRODUCTION

A. MOTIVATION

Ensuring a reliable and cost-effective electricity supply to consumers is critical in power systems. At the transmission system level, the application of reliability criteria has been the predominant reason to undertake network investments [1]. From an operational and planning perspective, improving continuity of supply involves a fundamental trade-off between higher reliability and the additional costs required to achieve it [2]. To analyze this trade-off in a systematic way, planning studies increasingly rely on optimization models that explicitly represent uncertainty and system security.

A large body of work has therefore developed stochastic decision-making frameworks for transmission planning and operation, ranging from probabilistic security assessment [3] to probabilistic security-constrained OPF formulations [4]. These approaches are appealing because they explicitly

The associate editor coordinating the review of this manuscript and approving it for publication was Atri Bera.

represent uncertainty induced by component outages and the system's behavior under contingencies, enabling planning decisions that reflect expected reliability performance and risk exposure [2]. However, despite their methodological maturity, the practical adoption of advanced probabilistic models remains limited in many jurisdictions. A key barrier is the availability and credibility of component-level reliability parameters, most notably outage (failure) and repair (recovery) rates of transmission assets. In practice, these parameters are frequently missing, incomplete, or not sufficiently reliable for planning-grade studies [5]. Even when historical records exist, they may not be representative of current conditions due to changes in asset management, reporting practices, network topology, operating policies, and exogenous drivers [6]. As a result, practitioners often rely on generic assumptions, expert judgment, or externally sourced parameters, which can yield reliability assessments that are misaligned with observed continuity metrics. This mismatch reduces the credibility of model-based results and limits their usefulness for investment decisions and regulatory discussions.

B. SCOPE AND ASSUMPTIONS

In this context, this paper proposes an alternative perspective: rather than attempting to directly estimate component-level reliability parameters from scarce or unreliable historical records, we leverage the information embedded in system-level continuity metrics, which are routinely monitored and reported by regulators, to infer reliability parameters through an inverse optimization approach.

The central premise of this work is that system-level continuity metrics contain informative signals about the effective reliability of transmission components when interpreted through a physically grounded operational model. To leverage this information, we adopt an calibration (inverse optimization) perspective [7], in which outage and repair rates are treated as unknown parameters to be inferred from observed continuity outcomes [8], [9] [10], while preserving consistency with network physics and operational constraints.

Accordingly, the scope of the proposed approach is to estimate a set of component reliability parameters that enable a probabilistic operational model to reproduce observed continuity indicators with improved consistency. This is inherently different from recovering true component-level parameters: any operational model used for planning is necessarily an abstraction of the real system, encompassing simplifications in network representation, the physical constraint set, and temporal aggregation [11], [12]. Under such modeling abstractions, multiple combinations of outage and repair rates can lead to very similar (or even identical) continuity-of-supply metrics, a property known as equifinality [13], [14]. As a result, the objective of calibration is not to identify a unique ground-truth parameter set, which in practice may not even exist, but rather to obtain parameters that are interpretable, physically plausible, and suitable for planning analyses within the adopted modeling framework.

We also clarify key assumptions and inherent limitations:

- The resulting inverse-calibration problem is generally non-convex; thus, global optimality guarantees are not the primary objective of the proposed methodology. Instead, emphasis is placed on obtaining stable and physically meaningful parameter estimates within a restricted domain of engineering plausibility. Specifically, the reliability parameters are optimized within predefined bounds derived from prior engineering knowledge, which serves two purposes: (i) it reduces the effective multimodality of the problem by excluding physically implausible regions of the search space, and (ii) it decreases the likelihood of obtaining spurious solutions. Within a sufficiently narrow and physically consistent bounded domain, the discrepancy between a local optimum and the best achievable fit is expected to remain small—though, for transparency, no formal guarantee of global optimality is claimed. The calibrated parameters obtained through this process represent an improvement over nominal industry values, as they reproduce observed continuity metrics more accurately.
- The approach relies on the availability and quality of system-level continuity metrics. Consequently, the calibrated parameters inherit the characteristics of the observed continuity data, which may depend on measurement practices, reporting conventions, and the level of spatial or temporal aggregation adopted by the system operator or regulator.
- Because the methodology produces parameters tailored to the chosen operational abstraction and the underlying dataset, extrapolation beyond the modeled conditions (e.g., substantially different operating policies, major structural changes in the system, or significantly different economic conditions) should be interpreted with care. In particular, the Chilean case study presented in this paper constitutes a retrospective validation based on the information available during the regulatory process leading to the 2020 transmission network reliability standard. Consequently, future applications of the proposed framework should update the technical, operational, and economic input data to reflect contemporary planning conditions, while the proposed inverse-calibration methodology itself remains unchanged.

Taken together, these considerations delineate the scope within which the proposed calibration perspective provides a practical pathway to enable reliability-oriented probabilistic planning when traditional data requirements cannot be satisfied.

C. CONTRIBUTIONS

In this context, this paper makes the following key contributions:

1) We propose an Inverse Probabilistic Security-Constrained Optimal Power Flow (Inverse PSC-OPF) framework to infer transmission component reliability parameters, specifically outage and repair rates, from observed continuity-of-supply metrics, while preserving consistency with network physics and operational constraints. This provides planning-grade reliability inputs in contexts where component-level outage data are missing, incomplete, or not sufficiently reliable.
2) We demonstrate the practical scalability of the proposed framework through a large-scale real-world application to the Chilean transmission system (≈2,200 lines/transformers and ≈2,400 buses). The study integrates the calibrated reliability parameters into a consistent chain of stochastic optimization models (Inverse PSC-OPF, forward PSC-OPF, and probabilistic transmission expansion planning), showing how calibrated reliability inputs enable computationally tractable reliability-oriented planning at realistic network scales. To address computational complexity, we combine complementary strategies (e.g., scenario structuring via machine learning, decomposition, and regularization), enabling the end-to-end workflow to be implemented on a realistic network.
3) The proposed framework has demonstrated direct real-world policy impact. The methodology and data pipeline presented in this paper directly informed the formulation of the Chilean transmission network reliability standard, becoming the first reliability standard developed through operations research and adopted by the Chilean National Energy Commission (NEC) in 2020. Consequently, the Chilean case study provides a retrospective validation of the proposed framework, demonstrating its ability to support real-world regulatory decision-making. In particular, the interruption-duration target identified by the proposed methodology was ultimately incorporated into the national regulation, achieving a balanced trade-off between supply continuity and transmission investment costs.

D. PAPER STRUCTURE

The remainder of this paper is organized as follows. Section II reviews the most closely related literature and positions the proposed contribution, inverse optimization for calibrating reliability parameters from observed continuity metrics, within existing work on reliability modeling, parameter estimation, and inverse problems in power systems. Section III establishes the conceptual framework, introducing the PSC-OPF as a reliability-consistent operational model and motivating the transition from forward to inverse approach. Section IV presents the proposed Inverse PSC-OPF formulation and the methodology to solve it, including the data preprocessing strategy and the metaheuristic solution approach. Section V describes the reliability-oriented transmission planning model that uses the calibrated parameters as inputs. Section VI presents the case study based on the Chilean transmission system. Section VII discusses the main results and their implications for continuity-of-supply assessment and standard setting. Finally, Section VIII concludes the paper and outlines directions for future work.

II. RELATED WORK

From a probabilistic perspective, improving the reliability levels of a power system through infrastructure investment should proceed up to the point at which the cost associated with such improvements exceeds their benefits [15]. However, cost–effectiveness analyses in investment decisions depend strongly on how the contingency probabilities used to quantify the cost of corrective actions are computed [16]. In principle, studies indicate that the probabilities used to generate random events should reflect not only the intrinsic characteristics of the equipment involved, but also external factors such as climatic conditions, which are unpredictable at planning time scales. These external factors can have a significant effect on failure probabilities and, consequently, on the expected cost of contingencies for a given operational dispatch [17]. More specifically, [2] shows that the probabilistic solution is a function of climatic conditions, through an exercise demonstrating that the levels of redundancy required in the network can decrease for systems located in regions with mild weather, since line failures are significantly less likely. Similarly, [18] reports that transmission-line failure probabilities may vary across regions and may even differ from one season to another, introducing dynamic behavior.

The most common way to compute contingency probabilities in the literature is through the reliability parameters of network assets. These data are obtained by statistically analyzing historical outage records of infrastructure [8]. This requires large volumes of data, recorded in a semi-automated way and accounting for dynamic behavior [19], [20]. This inevitably introduces significant sources of uncertainty that may lead to erroneous conclusions [19]. Existing reliability assessment tools typically use average failure-rate values for all components [21]. Other studies, such as [17] and [22], use multi-state weather models to calibrate reliability parameters. Efforts have also been made to calculate reliability parameters as a function of asset age [23], vegetation management [24], or combinations of characteristics such as vegetation density, lightning intensity, and wind intensity [25]. However, all of these models tend to be highly specific, which makes their generalized application difficult.

Data-driven models have also been developed to address the limitations of probabilistic approaches regarding how reliability parameters are used in contingency generation, particularly the assumption of perfect information. More specifically, [16] presents a distributionally robust optimization model to evaluate investments in distributed energy resources (DERs) and conventional network expansion, assuming ambiguous contingency probabilities by defining ambiguity sets that vary ± a given percentage around a nominal probability value. This allows indirect assessment of the importance of reliability parameters in transmission expansion planning. The results show that, due to data ambiguity, higher investment levels are required to protect the system against worst-case outcomes compared to approaches that assume perfect information. A similar analysis is conducted in [26], but without DER investment. The results show that equipment investments are strongly influenced by uncertainty in contingency probabilities and that, unlike fixed-probability approaches, ambiguous-probability formulations provide greater system coverage. While all these studies attempt to address the imprecision and lack of information in reliability parameters, they tend to be overly conservative, undermining industry credibility in real-world applications.

Given the above, academic efforts have been made to develop methods for obtaining reliability parameters that are credible to industry, i.e., that reflect the actual behavior of the system being modeled [5], [8], [9], [10], [27], [28]. More specifically, [27] presents an iterative process to adjust predicted continuity-of-supply metrics to historical values for a test distribution system, using sensitivity-based functions linking predicted metrics to reliability parameters. On the other hand, [8], [9], and [10], under the name of inverse power-system reliability evaluation, formulate an analytical model based on nonlinear algebraic equations to estimate unknown reliability parameters from specified reliability metrics. These analytical expressions are derived using state enumeration. However, the scope of these studies is limited to cases in which the number of unknown parameters equals the number of selected metrics, allowing the system of equations to be solved numerically. Finally, [5] and [28] perform reliability-parameter calibration by minimizing an error function between predicted and historical reliability metrics. However, the methods used have scalability issues and are heuristic in nature, and therefore are applied only to test systems.

In contrast to the above studies, which seek to adjust or calibrate reliability parameters to reflect actual system behavior, there also exists a body of work that treats reliability parameters as decision variables in optimization problems [29], [30], [31], [32], [33], [34], [35] with the goal of designing systems with improved reliability. More specifically, [29] identifies investments in distribution networks aimed at reducing failure rates and repair times, thereby decreasing forced outage rates and increasing system reliability. In [30], a method is presented to compute optimal reliability-metric values by modifying reliability parameters for a given load point, assuming allowable ranges for reliability indices and a cost per unit of failure-rate improvement representing investment in equipment. Similar approaches are developed in [34] and [35] for systems including both generation and transmission. All these works aim to determine the investments needed to achieve optimal reliability levels during system design, rather than to estimate reliability parameters that faithfully represent the existing system.

Reliability tracing models have also been proposed to assign reliability metrics to individual system components [36], [37], [38]. These studies quantify how much each component contributes to a given reliability metric. For example, if the metric is unserved energy (ENS), a simple allocation rule assigns responsibility to the components involved in the failed state that caused the ENS, with the amount allocated to each component proportional to its failure probability relative to the total probability of all failed components. This allows identification of weak components and supports reinforcement, redundancy, or meshing decisions.

To date, however, there exists no generic methodology capable of calibrating the nominal reliability parameters of power-system assets based on a set of observed reliability metrics. As shown by the above studies, only special cases exist, with limited scope, numerical tractability restricted to specific system structures, or heuristic approaches with poor scalability, applied only to test systems.

III. CONCEPTUAL FRAMEWORK: PSC-OPF AND INVERSE APPROACH

A. PSC-OPF AS A RELIABILITY-CONSISTENT OPERATIONAL MODEL

Probabilistic Security-Constrained Optimal Power Flow (PSC-OPF) [12] provides an operational framework in which power system operation is optimized under uncertainty induced by component outages. Unlike deterministic SC-OPF [39], which enforces feasibility for a predefined set of contingencies (e.g., N-1) without regard to their likelihood, PSC-OPF explicitly associates each contingency with a probability derived from the reliability parameters of network components. This allows the operational problem to internalize both the physical consequences of failures and their expected occurrence. In PSC-OPF, preventive actions (such as generation redispatch or reserve procurement) and corrective actions (such as post-contingency redispatch, network reconfiguration, or load shedding) are balanced through an expected-cost objective. Load curtailment is therefore permitted when it is economically justified by the low probability of certain severe contingencies, rather than being prohibited a priori. As a result, PSC-OPF produces not only optimal dispatch decisions but also system-level reliability outcomes such as expected energy not supplied, interruption durations, and interruption frequencies. Because PSC-OPF is built on a physically grounded power-flow model with network constraints, generator limits, and contingency-dependent feasibility, it provides a consistent mapping between component reliability parameters and observable continuity-of-supply metrics. For completeness, the full mathematical formulation of the forward PSC-OPF model used throughout this paper is provided in Appendix.

B. RELIABILITY PARAMETERS AS THE LINK BETWEEN COMPONENTS AND SYSTEM-LEVEL CONTINUITY

In PSC-OPF, the probabilities assigned to contingency states are functions of the failure and repair rates of transmission components. These reliability parameters determine how frequently specific network elements are unavailable and, consequently, how often the system operates under degraded topologies. Through this mechanism, component-level reliability directly affects the expected occurrence of congestion, load shedding, and other corrective actions. System-level continuity-of-supply metrics, such as unserved energy, interruption duration, and interruption frequency, are therefore not exogenous quantities in PSC-OPF, but outputs of the operational model driven by the underlying reliability parameters. Changing failure or repair rates alters the probability distribution over contingencies, which in turn changes the expected operational outcomes produced by the PSC-OPF. This forward mapping from reliability parameters to continuity metrics is highly nonlinear and mediated by network physics, operational constraints, and corrective control decisions. As discussed in the literature review, this complexity, combined with data limitations, makes it difficult to specify reliability parameters a priori in a way that is consistent with observed system performance.

C. FROM FORWARD PSC-OPF TO INVERSE APPROACH

The calibration problem addressed in this paper arises from inverting the forward PSC-OPF mapping. Instead of treating failure and repair rates as fixed inputs used to compute expected reliability outcomes, we treat observed continuity-of-supply metrics as given and seek the set of reliability parameters that make the PSC-OPF reproduce them as closely as possible. Formally, this leads to an inverse optimization problem in which the PSC-OPF acts as a constraint linking decision variables (the reliability parameters) to observable outputs (continuity metrics such as unserved energy or interruption indices). Because PSC-OPF is itself an optimization problem, the resulting inverse formulation is a bilevel or nested structure, where reliability parameters affect the solution of the forward operational model. This perspective distinguishes the proposed approach from both traditional statistical estimation of reliability parameters and heuristic calibration techniques. The inverse PSC-OPF enforces physical and operational consistency by construction, since any candidate parameter set must be compatible with feasible power-system operation under contingencies. At the same time, it allows system-level performance data to directly inform the estimation of component-level reliability inputs. The next section formalizes this inverse-calibration framework and presents the mathematical formulation of the Inverse PSC-OPF.

IV. THE PROPOSED METHODOLOGY FOR CALIBRATION VIA INVERSE OPTIMIZATION

In this section, we formalize the calibration framework proposed in this paper. We first state the inverse PSC-OPF problem, which seeks to infer transmission-component reliability parameters from observed continuity-of-supply metrics while preserving consistency with network physics and operational constraints. We then show how this inverse problem is implicitly defined through the optimal solution of a forward probabilistic security-constrained optimal power flow (PSC-OPF), leading to a bilevel optimization structure. Next, we provide the necessary definitions for power-system reliability modeling and the analytical expressions of the continuity-of-supply metrics of interest. We then describe a data preprocessing step based on clustering, which improves tractability and mitigates overfitting. Finally, we present the solution strategy adopted to solve the resulting nonconvex inverse-optimization problem.

A. INVERSE PSC-OPF FORMULATION

Let r denote the vector of transmission-component reliability parameters to be calibrated. In this paper, r includes the outage (failure) and repair (recovery) rates of all relevant network assets. Let q_j be the observed value of a continuity-of-supply metric for node or group of nodes j, obtained from historical operation over a given assessment horizon. For any candidate parameter vector r, the forward PSC-OPF model produces a corresponding set of model-implied continuity metrics $h_j(r)$, which are induced by the optimal operational decisions and the contingency probabilities determined by r. In this context, the inverse-calibration problem is formulated as the minimization of an aggregate mismatch between modeled and observed continuity metrics:

$$\min_{r} \quad \Phi(\varepsilon) + \Omega(r) \tag{1a}$$

$$r^L \leq r \leq r^U \tag{1b}$$

where $\varepsilon = (\varepsilon_j)_{j \in J} = (h_j(r) - q_j)_{j \in J}$ is the vector of calibration errors, $\Phi(\cdot)$ is a norm-based loss function measuring the discrepancy between model-implied and observed continuity indicators (e.g., based on an l_1, l_2, or weighted norm), $\Omega(r)$ is a regularization term used to promote stability when the inverse problem is ill-conditioned or degenerate, and to ensure physical plausibility, the reliability parameters r are restricted to an engineering-feasible domain, where r^L and r^U define lower and upper bounds for the outage and repair rates based on technical knowledge and prior information.

The mapping $h_j(r)$ is not available in closed form; it is induced by the optimal solution of a forward stochastic operational model. For a given reliability vector r, the PSC-OPF evaluates system operation over a set of contingencies S, where each contingency $s \in S$ occurs with probability $p_s(r)$ determined from the component-level reliability parameters.

Let x_s denote the set of operational decision variables under contingency s. The forward PSC-OPF can be written as:

$$x^*(r) \in \arg\min_{x} \quad \sum_{s \in S} p_s(r) \cdot C_s(x_s) \tag{2a}$$

$$\text{s.t.} \quad x_s \in X_s, \quad \forall s \in S \tag{2b}$$

Given the optimal solution $x^*(r)$, the model-implied continuity metrics are obtained through:

$$h_j(r) = H_j\big(x^*(r),\, p(r)\big) \tag{3}$$

Combining the inverse objective with the forward operational embedding yields the Inverse PSC-OPF:

$$\min_{r,x,\varepsilon} \quad \Phi(\varepsilon) + \Omega(r) \tag{4a}$$

$$\text{s.t.} \quad \varepsilon_j = h_j(r) - q_j, \quad \forall j \in J \tag{4b}$$

$$x \in \arg\min_{\tilde{x}} \sum_{s \in S} p_s(r) \cdot C_s(\tilde{x}_s) \tag{4c}$$

$$\text{s.t.} \quad \tilde{x}_s \in X_s, \quad \forall s \in S \tag{4d}$$

$$r^L \leq r \leq r^U \tag{4e}$$

This bilevel formulation highlights the core methodological contribution of this paper: reliability parameters are inferred by enforcing consistency between observed continuity-of-supply metrics and the outcomes of a physically grounded probabilistic operational model. However, this structure makes the inverse problem inherently nonconvex. The non-convexity arises from two sources: first, the contingency probabilities $p_s(r)$ are nonlinear functions of the reliability parameters r, as detailed in the following subsection; and second, these probabilities multiply the operational cost variables of the second level, giving rise to bilinear terms in the combined objective function.

The inverse PSC-OPF does not aim to identify a unique true set of failure and repair rates. Under any operational abstraction, multiple reliability vectors may produce nearly identical continuity metrics. The goal is instead to obtain a set of reliability parameters that is consistent with observed continuity behavior, physically plausible, and suitable for reliability-oriented planning and policy analysis within the adopted modeling framework.

The following subsections specify the continuity metrics $h_j(\cdot)$, the data preprocessing strategy and the numerical solution method used to solve the resulting nonconvex inverse optimization problem, and an illustrative example on a controlled instance to highlight the value of the calibration process and its impact on investment decisions.

B. ANALYTICAL EXPRESSIONS OF THE SUPPLY CONTINUITY METRICS h_j

We use a Markov process to represent the transitions between the different states of the system, which allow us to determine the h_j metrics as explained in [40]. That is, for each asset i, the availability A_i and unavailability U_i are calculated using its reliability parameters, specifically the outage λ_i and repair μ_i rates, through the following expressions:

$$A_i = \frac{\mu_i}{\lambda_i + \mu_i} \tag{5a}$$

$$U_i = \frac{\lambda_i}{\lambda_i + \mu_i} \tag{5b}$$

Then, the probability p_s of each system state s (or scenario s) is calculated as follows:

$$p_s = \prod_{i \in \mathcal{B}_s^{up}} A_i \cdot \prod_{i \in \mathcal{B}_s^{dw}} U_i \tag{6a}$$

where $\mathcal{B}_s^{up}$ and $\mathcal{B}_s^{dw}$ are the sets of available and unavailable components, respectively, under the system state s. In this paper, we use the following h_j metrics: System Average Interruption Frequency Index (SAIFI) [occurrences], System Average Interruption Duration Index (SAIDI) [hours], and Expected Energy Not Supplied (EENS) [MWh], whose analytical expressions are:

$$\text{SAIDI}_j = \sum_{s \in \mathcal{S}_j^{ls}} p_s \cdot T \tag{7a}$$

$$\text{SAIFI}_j = \sum_{s \in \mathcal{S}_j^{ls}} F_{sj} = \sum_{s \in \mathcal{S}_j^{ls}} \sum_{k \in \mathcal{S}_j^{0}} p_k \cdot r_{ks} \tag{7b}$$

$$\text{EENS}_j = \sum_{s \in \mathcal{S}_j^{ls}} p_s \cdot L_{sj} \cdot T \tag{7c}$$

Notice that T refers to the duration of the representative operating condition (e.g., if a year is represented by a single timeslice, T equals 8760 hours), F_{sj} the frequency at which the system state s is reached from any other state without load shedding $\mathcal{S}_j^0$ in node j, r_{ks} the transition between states k and s by using λ_i or μ_i as appropriate, and L_{sj} the load shedding for each system state s and node j. The states with and without load shedding $\mathcal{S}_j^{ls}$ and $\mathcal{S}_j^0$, together with the amounts of load shedding L_{sj}, will be determined by two OPF models, as explained later (Figure 1).

C. IMPLEMENTATION STRATEGY: PREPROCESSING DATA AND THE SOLUTION STRATEGY

The proposed methodology is applied through a two-step process. The first step involves preprocessing data, where the machine learning technique known as *decision trees* is used to cluster demand nodes and network assets into groups. Given that outages are infrequent, historical records can be inaccurate or biased due to the limited dataset. Therefore, we use groups rather than individual data avoiding overfitting to individual (and potentially inaccurate) values. Additionally, clustering data into groups enhances the model's tractability.

The second step involves solving the inverse PSC-OPF model, described in equations (4a) - (4e), using a metaheuristic approach. This approach determines the reliability parameters of network components that replicate the supply interruption levels observed in historical data. Below, we explain these steps in more detail.

1) CLUSTERING BUSES AND ASSETS

Buses: We aim to form Ψ groups of (comparable) buses sharing similar topological and electrical features, and where the variance of supply continuity metrics within each cluster ψ is minimal. To achieve this, we use *decision trees*, which predict the value of a target variable (in this case, a supply continuity metric like SAIFI, SAIDI or EENS) by learning simple decision rules inferred from data features. These rules shape the branches of the decision tree, ultimately defining each cluster. We use the following four features to characterize each bus:

- Radiality: Indicates whether the node is connected to a radial or meshed part of the network. A node's connection is considered radial if there is a single branch or circuit connecting it to the rest of the system, meaning there are no loops. In the radial case, this metric reflects the distance between the node and the closest meshed piece; otherwise, it is zero.
- Connectivity: The number of branches that are incident to the node (i.e., degree or valency).
- Voltage: The voltage level of the node.
- Distributed generation: The aggregated capacity embedded in the node.

We expect nodes connected to a meshed piece of the transmission network, with high connectivity and voltage levels, and a larger capacity of distributed generation, to feature improved supply continuity levels. Other features could be used as well, depending on the case and available data. This approach also enhances model tractability as it reduces the number of h_j metrics.

Assets: The lack of richer outage data may lead to substantially different reliability parameters across network components, even for comparable ones. This motivates sharing the same outage and repair rates (per unit of length, in the case of lines) within assets of the same class. We define a class according to the component type, its voltage level, and location (e.g., transmission lines of 220 kV located in a given zone are assumed to feature the same reliability data). In our study, this feature is highly desirable for the power industry as differences in reliability data for similar assets are difficult to justify in practice. This approach also enhances model tractability as it reduces the number of outage and repair rates to be calibrated. Depending on the application, these classes may be defined according to other features as well (e.g., the aging of components).

2) THE SOLUTION STRATEGY TO SOLVE THE INVERSE OPTIMIZATION PROBLEM

We use three concatenated optimization programs to solve (4a) - (4e) and determine the network components' outage and repair rates that reproduce the historical levels of the supply continuity metrics (Figure 1). First, we run a SC-OPF problem to determine the pre- and post-contingency operation for each timeslice, aiming to replicate the system operator's dispatches of generators for every operating condition. Over this pre-contingency operation fixed, we simulate a higher set of contingencies to identify in which scenarios load is disconnected and by how much, which is necessary to determine $h_j(r)$ metrics (e.g., SAIDI, SAIFI and EENS, for different groups of nodes). Finally, we use an Separable Natural Evolution Strategy metaheuristic (SNES) to solve (4a) - (4e), which is suitable for non-convex problems like ours.

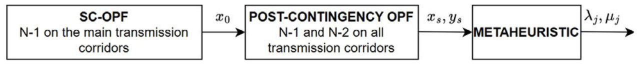

FIGURE 1. Calibration process diagram.

The metaheuristic starts with an initial population of individuals, each representing a solution to the inverse problem (i.e., a set of λ_i and μ_i values for each asset class), randomly generated within a prespecified range. Subsequently, through crossover and mutation operators, new individuals are created, and the initial population evolves according to a selection criterion based on a fitness function f_{sc} (namely, the inverse problem's objective) that captures the adjustment errors ϵ_j relative to the historical metrics q_j. The process stops when the errors are less than or equal to a given tolerance or a maximum number of iterations is reached.

Specifically, the calibration process considers reliability metrics at three complementary aggregation levels: systemwide indicators, load-weighted nodal indicators, and cluster-level indicators. The resulting L_1-based calibration objective function is formulated as:

$$f_{sc} = \alpha_{\text{sys}} \cdot \left\|\varepsilon^{\text{sys}}\right\| + \alpha_{\text{lw}} \cdot \left\|\varepsilon^{\text{lw}}\right\| + \sum_{\psi \in \Psi} \alpha_{\psi}^{\text{clust}} \cdot \left\|\varepsilon_{\psi}^{\text{clust}}\right\|, \tag{8}$$

where $\|\varepsilon^{\text{sys}}\|$ denotes the systemwide discrepancy, $\left\|\varepsilon^{\text{lw}}\right\|$ represents load-weighted nodal discrepancies, and $\left\|\varepsilon_{\psi}^{\text{clust}}\right\|$ corresponds to the discrepancies associated with cluster $\psi \in \Psi$. The coefficients α_i are weighting parameters used to balance the contribution of each calibration component. The calibration objective adopts an L_1-norm formulation as a computational modeling choice to preserve a linear objective function, thereby maintaining the tractability of the large-scale inverse calibration problem. In contrast, formulations based on squared errors would introduce quadratic terms requiring additional approximations, significantly increasing the computational burden. Therefore, the adopted L_1 formulation should be interpreted as a computational trade-off that enables the proposed framework to be applied to realistic transmission systems.

D. ILLUSTRATIVE EXAMPLE HIGHLIGHTING THE VALUE OF THE CALIBRATION PROCESS

The purpose of this section is to illustrate how the use of reliability parameters inconsistent with the actual behavior of the transmission system may distort reliability-oriented planning decisions. Indeed, if reliability parameters do not

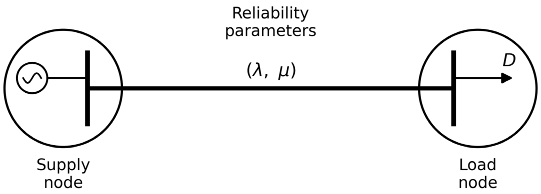

FIGURE 2. Test system.

adequately reproduce observed supply continuity metrics, the probabilities associated with transmission contingencies become biased, potentially leading to overinvestment or underinvestment in transmission infrastructure.

To illustrate this effect, a numerical example is presented in which system operation is simulated for a given network topology using both a detailed model and a simplified model at hourly resolution. The detailed model represents the reference benchmark used to compute the observed supply continuity metrics under the nominal reliability parameters. By contrast, the simplified model represents the reduced operational representation typically available in practical planning studies. Due to its lower temporal resolution, the simplified model produces reliability metrics that differ from the observed benchmark values, thereby motivating a calibration process for the nominal reliability parameters in order to compensate for this modeling discrepancy. Without loss of generality, the only supply continuity metric considered in this illustrative example is *EENS* [MWh/year].

Accordingly, Figure 2 considers a simple two-node system: one generation node with 100 [MW] of capacity and one demand node. Both nodes are connected through a transmission line that may fail, and whose nominal reliability parameters, namely failure and repair rates, are $\lambda = 0.05$ [times/year] and $\mu = 5$ [times/year], respectively. This gives rise to a single possible contingency s, with occurrence probability $p_s = \lambda/(\lambda + \mu)$.

For each model, each post-contingency state is simulated using an OPF model, disabling the corresponding network element. On the one hand, the detailed model considers a time resolution of two time blocks $T = \{1, 2\}$, with demands of 50 and 100 [MW], respectively, which together represent one hour of operation (30 minutes per block). On the other hand, the simplified model considers a single time block $T = \{1\}$, with peak demand of 100 [MW], also representing one hour of operation. For each block t, at load node j, and under contingency s, the value $L_{t,s,j}$ is determined, which, together with the nominal reliability parameters, allows the observed supply metric EENS_j^{obs} to be computed for load node j and the operating hour considered. The resulting value can then be extrapolated to one year of operation by multiplying by 8760 [h/year]. The formula used to compute EENS_j^{obs} is based on (7c):

$$\mathrm{EENS}_j^{obs} = \sum_{t\in T} \frac{1}{|T|} \cdot \sum_{s\in S_j^{ls}} p_s \cdot L_{t,s,j} \cdot 8760. \tag{9}$$

The resulting values for the detailed and simplified models are 6504.94 [MWh/year] and 8673.27 [MWh/year], respectively.

It can be seen that the simplified model yields a higher value than the detailed model because the former uses only one peak-demand time block. To quantify the degree of discrepancy, the absolute value is used as the error function, leading to the following inverse optimization problem:

$$\min_{\Delta\lambda,\Delta\mu>0} \sum_{\forall j\in J} \left| \mathrm{EENS}_j^{cal}(\Delta\lambda, \Delta\mu) - \mathrm{EENS}_j^{obs} \right|, \tag{10}$$

which, for this example, can be written as:

$$\min_{\Delta\lambda,\Delta\mu>0} \left| 8760 \cdot \sum_{\forall s\in S_j^{ls}} \frac{\lambda\cdot\Delta\lambda}{\lambda\cdot\Delta\lambda + \mu\cdot\Delta\mu} \cdot L_{sj} - \mathrm{EENS}_j^{obs} \right|, \tag{11}$$

where j represents the load node of interest, and $\mathrm{EENS}_j^{cal}(\Delta\lambda, \Delta\mu)$ denotes the mathematical expression used to compute the metric under analysis. The optimization results, namely $\Delta\lambda = 3.2837978$ and $\Delta\mu = 4.38935019$, yielding

$$\mathrm{EENS}_j^{cal}(\Delta\lambda, \Delta\mu)^* = 6504.94,$$

indicate that a perfect calibration process (zero discrepancy) has been achieved.

To analyze the impact of calibration on planning decisions, a simple transmission expansion problem is then considered. The transmission corridor may be reinforced through an additional backup capacity F [MW], with investment cost $c^{Inv} = 8.5$ [USD/MW]. Unserved energy is penalized using $\mathrm{VOLL} = 1000$ [USD/MWh].

Under nominal reliability parameters, the contingency probability is sufficiently high to justify full redundancy investment:

$$F^{*,nom} = 100 \text{ [MW]}.$$

However, when calibrated reliability parameters are used, the effective outage probability decreases and the investment becomes economically unattractive, leading to:

$$F^{*,cal} = 0 \text{ [MW]}.$$

This example shows that the use of uncalibrated reliability parameters may significantly distort transmission planning decisions by misrepresenting the effective value of reliability improvements. Consequently, reliability-oriented planning models should rely on calibrated reliability parameters consistent with observed supply continuity metrics in order to produce coherent investment signals and realistic expansion portfolios.

V. THE APPLICATION: NETWORK INVESTMENTS FOR RELIABILITY ENHANCEMENTS

A. PURE COST-BENEFIT BALANCE

In this work, the calibrated reliability parameters are used to determine the optimal set of investments in transmission infrastructure to mitigate the impact of outages on system operations, thereby improving the supply continuity levels perceived by consumers. To achieve this, the PSC-OPF formulation (see Appendix) can be readily extended to include network investment decisions in its first stage [41], [42], thus modifying pre- and post-contingency actions by increasing transmission capacity. In addition, the investment costs must be considered in the objective function of the problem. This extended model is stated in [2]. Given the application of this formulation to a very large-scale instance, we employ decomposition and regularization techniques, along with additional methods detailed below.

For Benders decomposition, we follow the approach in [43], where investment and pre-contingency operation decisions are included in the master problem, while the post-contingency operations are handled by a set of subproblems that can be solved in parallel. Each subproblem determines post-contingency operations given the investment and pre-contingency operation proposals determined by the master problem.

Regarding the regularization technique, we apply a variant of the method proposed by [44], which introduced quadratic regularization as a term in the objective function that penalizes deviations of state variables from their values in the previous iteration. This term diminishes as iterations progress. Our variant differs in that we use the absolute-value distance instead of the Euclidean distance to maintain linearity, as explained in [45]. Additionally, computational complexity is further reduced by decoupling network investment decisions in radial and meshed transmission assets, as the interaction between both is minimal.

B. TARGET SUPPLY CONTINUITY LEVELS

Another feature of our model is the inclusion of SAIDI metric as linear function of EENS within the set of constraints. Specifically, for each demand node $n \in N$, we construct a node-specific linear approximation of the form $\text{SAIDI}_n \approx \text{coef}_n \cdot \text{EENS}_n$, where coef_n is estimated independently for each node through a separate linear regression using historical annual observations of $(\text{EENS}_n, \text{SAIDI}_n)$ pairs. This yields a distinct coefficient for every demand node, thereby capturing the local relationship between EENS and SAIDI, which naturally reflects differences in demand magnitude and interruption characteristics across the network. Consequently, high-demand nodes typically exhibit smaller values of coef_n, whereas low-demand nodes typically exhibit larger values. The nodal SAIDI constraint is then incorporated into the investment model as:

$$\text{SAIDI}_n = 8760 \cdot \sum_{s \in S} p_s^* \cdot L_{sj} \cdot \text{coef}_n \leq \overline{\text{SAIDI}}_n, \quad \forall n \in N \tag{12}$$

where p_s^* denotes the optimal contingency probability derived from the calibrated reliability parameters (see Section IV), and $\overline{\text{SAIDI}}_n$ is the maximum allowable interruption duration at node n, representing the supply continuity target set by the regulator.

The proposed EENS-to-SAIDI mapping should be interpreted as a computational modeling approximation introduced to preserve the tractability of the large-scale transmission expansion planning problem. Although the exact relationship between EENS and interruption duration is inherently nonlinear, the proposed nodal approximation provides a practical representation that enables the incorporation of supply continuity targets within a realistic large-scale optimization framework.

Thus, the model not only identifies the portfolio of network investments that optimally balances the costs of investments and unsupplied demand, but it also determines the portfolio of network investments that achieves target supply continuity levels in each node at minimum cost. This approach serves to analyse the Chilean energy policy outlined in the country's Energy Roadmap [46], which sets explicit annual outage duration limits for each node.

It is important to mention that the solution strategy adopted in this work is based on a standard Benders decomposition framework. Extending this framework to directly enforce nodal supply continuity constraints would require a different and substantially more sophisticated Benders decomposition variant, resulting in a significantly higher computational burden. Therefore, to identify network enhancements that satisfy the prescribed nodal supply continuity targets, we first determine the optimal investment portfolio from a pure cost-benefit perspective (as described in the previous section). With these assets fixed, we then solve the monolithic investment model (without decomposition) including the nodal supply continuity constraints to identify any additional network reinforcements required. This two-step solution strategy represents a computational trade-off that enables the proposed methodology to be applied to a realistic transmission system while maintaining tractable solution times.

VI. CASE STUDIES AND INPUT DATA

We run one central case study and several sensitivities. The central case study determines the optimal set of network investments justified due to a cost-benefit balance between (i) the investment (including maintenance) costs of the new network infrastructure and (ii) the corresponding reductions in the expected cost of energy not supplied (i.e., supply continuity improvements). Then, we run several sensitivities that, rather than freely balancing these costs, impose a given supply continuity target for all nodes, determining the optimal network enhancements that comply with such target. We run the model for a wide range of targeted values of SAIDI, from 0.15h to 40h. The same SAIDI value is applied to all demand nodes simultaneously. We use SAIDI as a targeted metric of continuity of supply as it is consistent with the energy policy agenda in Chile. Before running the above case studies, we calibrate network components' reliability parameters using the method proposed in this paper, demonstrating that the model can deliver credible results for the power industry.

It is important to emphasize that the Chilean case study presented in this paper constitutes a retrospective validation of the proposed methodology. Consequently, all technical, operational, and economic input data correspond to the information available during the regulatory process that ultimately led to the adoption of the 2020 Chilean transmission network reliability standard. As such, the objective of this case study is to validate the proposed framework in a real-world regulatory setting rather than to derive an updated transmission expansion plan under current planning conditions.

The most relevant considerations in terms of input data, assumptions, and modeling are:

- We use a 2400-bus representation of the Chilean transmission system (545 demand nodes, 450 generators, 1298 lines, and 869 transformers).
- Demand per node, parameters of generators (capacities and costs), and the network topology mentioned above correspond to those used and published by the Chilean system operator [47].
- Investment and maintenance costs of network components are taken from the Regulated Asset Value report published by the regulatory authority for tariff purposes [48].
- The value of the lost load is equal to $12,960/MWh [49].
- For potential investments, we consider candidate network components so every branch in the network complies with the N-1 redundancy criterion: 1,002 candidate lines and 225 candidate transformers. Today, only a fraction of the transmission network complies with it.
- We restrict our study to contingencies consisting of single or double outages (for the case of lines in the same circuit). This is motivated by the nature of potential investments considered.
- Prior estimates associated with the reliability parameters of network components are taken from estimations by the Chilean system operator. We only consider data associated with forced outages under milder events as planned outages and extreme events are ignored when SAIDI, SAIFI, and EENS are measured [50].
- The network companies report SAIDI, SAIFI, and EENS in all demand nodes to the Chilean regulatory office. We use the data available between 2012 and 2018. However, calibration is performed based on SAIDI and SAIFI, which correspond to the duration and frequency of interruption indicators used in the regulatory assessment of supply quality in Chile. Although EENS is relevant in planning contexts, it is not included in the objective function in order to maintain consistency with the indicators used in regulatory practice.
- All studies are carried out for the present system condition (2019) to avoid investments due to demand growth. Hence, investments can be justified only due to reliability benefits (i.e., post-contingency congestion relief). We also add further constraints in the pre-contingency operation to mimic actual power transfer limits applied by the system operator and thus obtain credible results for the power industry [51].

TABLE 1. Final values of the calibration objective components.

Calibration metric	Relative error (%)
Systemwide SAIDI error	16.76
Weighted SAIDI error	3.05
Weighted SAIFI error	0.004
Cluster-level SAIDI error	0.25
Cluster-level SAIFI error	146.67

VII. RESULTS AND DISCUSSION

A. CALIBRATION

As outlined in Section IV, we cluster the network buses (or nodes) into groups based on their features such as radiality, connectivity, voltage and volumes of distributed generation in different locations of the system. Then, we calibrate the reliability data for each asset class to match the modeled and observed supply continuity data, specifically the systemwide SAIDI, and the SAIDI and SAIFI of each node group.

The results were obtained using the SNES metaheuristic with a maximum budget of 8000 objective function evaluations, corresponding to approximately 470 evolutionary generations. A global sampling standard deviation of 0.05 was adopted. The weighting parameters of the calibration objective function were set to $\alpha_{\text{sys}} = 4$, $\alpha_{\text{lw}} = 4$, and $\alpha_{\psi}^{\text{clust}} = 2$. Higher weights were assigned to the systemwide and load-weighted terms in order to prioritize the accurate reproduction of the global reliability behavior of the system, while cluster-level discrepancies were incorporated with lower weights to preserve spatial representativeness without excessively biasing the calibration toward local variations. The complete optimization process required approximately 60 hours of computational time on the employed computing platform, equipped with an Intel Core i9-10980HK processor running at 2.40 GHz, 32 GB of RAM, and a 64-bit operating system.

To further assess the quality of the obtained solution, Table 1 reports the relative errors associated with each component of the calibration objective function, including the systemwide SAIDI error, the load-weighted SAIDI and SAIFI discrepancies, and the cluster-level SAIDI and SAIFI errors.

The results demonstrate that the proposed methodology achieves a satisfactory agreement between modeled and observed reliability indicators, reaching a final calibration objective value (fitness) of 3.73. In particular, the calibration accurately reproduces the load-weighted SAIDI and SAIFI indicators, while also providing a very close approximation of the cluster-level SAIDI patterns throughout the network. Greater discrepancies remain in the cluster-level SAIFI indicators, reflecting the difficulty of simultaneously reproducing local interruption frequencies across geographically diverse areas using a limited set of calibration parameters. Nevertheless, the calibrated failure and repair rates provide a coherent and representative characterization of the overall reliability performance of the system. Although further improvements may still be possible through additional objective function evaluations, the optimization process was intentionally terminated once a satisfactory compromise between calibration quality and computational burden was achieved.

The resulting calibrated failure and repair rates are depicted in Figure 3, showing that transformers have a lower failure frequency than lines. Additionally, as expected, lines with higher voltages fail less frequently since higher voltage towers are more robust. Figure 3 also shows significant variance in the reliability performance of network assets within the same class, suggesting that local characteristics (e.g., environment and climate) and their particular state of health (due to aging and maintenance policies) significantly affect reliability data. The large differences between the calibrated rates and their prior estimates highlight the importance of our proposed calibration method, as without it, a single prior value would be used for all assets in the same class, potentially leading to inaccurate assessments.

To assess the effectiveness of the proposed calibration framework, different metaheuristic optimization methods were tested, including CDE, JADE, and SHADE. Figure 4 compares the convergence behavior of these approaches in terms of the best-so-far fitness value as a function of the number of objective function evaluations, while Table 2 summarizes their final objective values and computational performance. For comparison purposes, all methods were evaluated using a stopping criterion of 2500 objective function evaluations due to the high computational burden associated with the repeated probabilistic reliability calculations required to evaluate the calibration objective function.

Under this common evaluation budget, SNES achieved the best overall calibration performance, attaining the minimum final fitness value (4.94). JADE and SHADE also achieved competitive results, converging to low final objective values (5.54 and 5.52 respectively), whereas CDE remained noticeably less competitive (15.59). However, important differences can still be observed in the convergence behavior of the evaluated methods. SNES exhibited a smoother and more stable convergence trajectory, consistently reducing the objective value across generations. By contrast, JADE and SHADE displayed a more abrupt convergence pattern, characterized by significant improvements during later stages of the search process, while CDE exhibited slower and less stable convergence dynamics throughout the optimization process. It is also worth noting that, once low-fitness regions are reached, further objective value reductions become increasingly difficult. Nevertheless, even relatively small fitness improvements in these regions may translate into meaningful reductions in the calibration errors reported in Table 1.

TABLE 2. Performance comparison of the evaluated metaheuristic optimization methods.

Method	Final fitness	Evaluations	Runtime (h)
SNES	4.94	2500	30.50
CDE	15.59	2500	26.37
JADE	5.54	2500	33.60
SHADE	5.52	2500	25.61

These results suggest that methods capable of maintaining adaptive and robust exploration mechanisms are particularly effective for the proposed calibration problem, which is characterized by a highly nonconvex and degenerate optimization landscape. Unlike differential evolution-based methods such as CDE, JADE, and SHADE [52], SNES evolves a probabilistic search distribution rather than individual candidate solutions. This allows the algorithm to adapt the search process using statistical information from the population as a whole, promoting smoother exploration of the parameter space and reducing sensitivity to local variations between equivalent solutions. Such characteristics are especially advantageous in the proposed reliability calibration framework, where multiple combinations of failure and repair rates can produce similar reliability indicators, leading to broad regions of near-equivalent solutions in the search space.

B. BALANCING INVESTMENT COSTS AND RELIABILITY ENHANCEMENTS

After calibrating the failure and repair rates, we proceed to enhance the transmission network. The optimal solution for the transmission expansion planning problem, which balances investment and unsupplied energy costs, involves \$24.2M in annuitized investment costs. This results in \$97.5M in savings from the expected costs of energy not supplied, yielding a net benefit of \$73.3M. Notably, the expected energy not supplied is halved, and the systemwide SAIDI and SAIFI are significantly reduced by 48% and 25%, respectively. About 65% of the investment costs are allocated to building new lines, covering approximately 1000 km. Additionally, the model installs about 1.7 GW in 25 new transformers. These results are shown in Table 3.

From a policymaker's perspective, a critical issue with the above optimal solution is the uneven distribution of reliability levels across the network. Figure 5 shows the distribution of nodal SAIDIs before and after the investments. Although there is a significant improvement in the systemwide SAIDI (a 48% reduction), local SAIDI remains poor for several buses. Dots with high SAIDI represent nodes usually located far from the main meshed system and with small demand levels. In these areas, installing redundancies is costlier than the corresponding savings in the expected cost of energy not supplied. We address this "equity" problem in the next section.

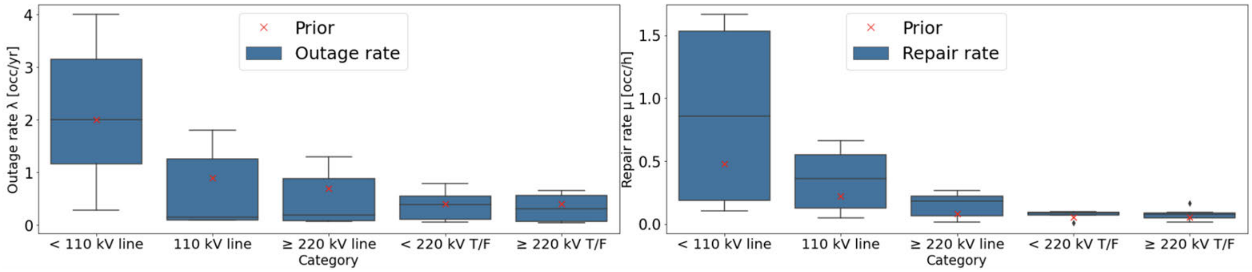

FIGURE 3. Failure rates and repair rates of component classes (per 100 km lines and transformers; T/F refers to transformers). The given prior estimates are presented in red color.

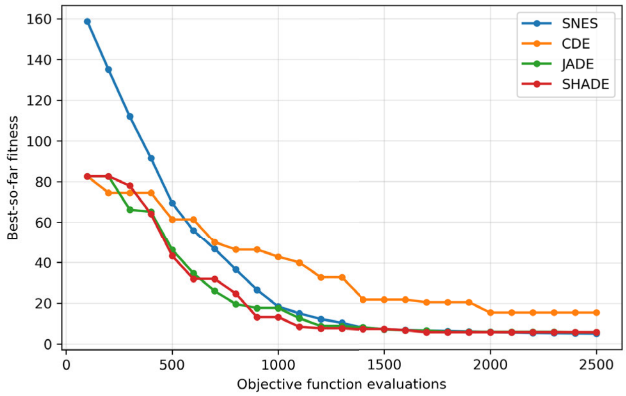

FIGURE 4. Comparison of convergence performance among different metaheuristic optimization methods.

TABLE 3. Results of optimal investments (M$ refers to millions of dollars).

Investments in lines	
No. lines	48
Aggregated length [km]	1,041
Capacity [MW]	2,316
Investment cost (lines) [M$/yr]	15.7
Investments in transformers	
No. transformers	25
Capacity [MW]	1,765
Investment cost (transformers) [M$/yr]	8.5
Cost–benefit balance	
Investment cost (total) [M$/yr]	24.2
Expected cost of energy not supplied (reduction) [M$/yr]	97.5
Expected net benefit [M$/yr]	73.3
Systemwide supply continuity metrics (before - after investments)	
EENS [GWh/yr]	(14 - 7)
SAIDI [h/yr]	(2.3 - 1.2)
SAIFI [occ/yr]	(1.3 - 1)

C. RELIABILITY-CONSTRAINED INVESTMENTS: IMPROVING WORST-SERVED AREAS

In this section, we study target reliability levels per node by enforcing an upper bound on the SAIDI levels across all nodes. Figure 6 shows the annuitized investment costs associated with imposing different upper bounds on SAIDI.

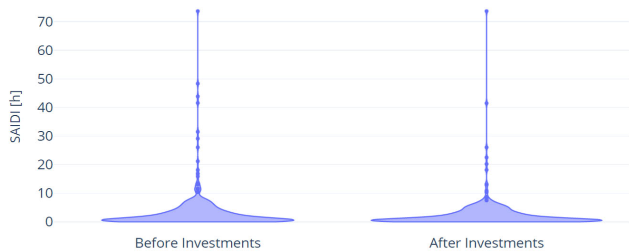

FIGURE 5. Distribution of SAIDI across the nodes pre- and post-investment.

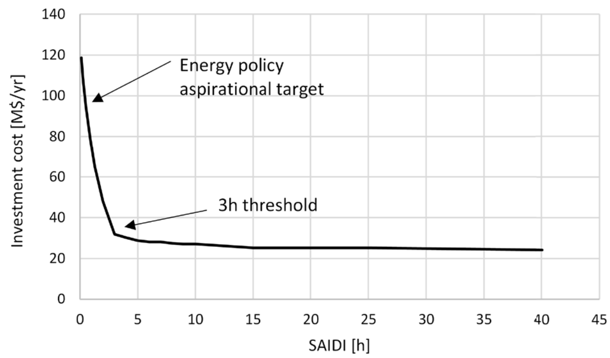

FIGURE 6. Annuitized investment cost as a function of SAIDI's upper bound applied on all nodes.

Expectedly, more stringent reliability levels drive higher costs. For instance, the aspirational energy policy target of 0.5 hours leads to an investment cost of $95.1M per year, significantly higher than the optimal investment cost found in the previous section ($24.2M). Interestingly, imposing a SAIDI limit of up to 3 hours on every node appears to be a reasonable compromise between costs and policy aspirations, as investment costs escalate considerably below this threshold.

Finally, it is essential to highlight that improving reliability beyond the levels shown in Table 3 and imposing arbitrary reliability targets may result in disproportionately high network costs and thus tariffs. Additionally, our results demonstrate that these improvements are mainly undertaken in rural areas, where increasing tariffs may be particularly complicated due to the consumers' socio-economic backgrounds. Cross-subsidies may likely be needed to support more equitable and fairer solutions regarding the distribution of supply continuity levels among network users.

VIII. CONCLUSION AND IMPACTS OF THIS WORK

This paper introduces a novel inverse optimization approach for the PSC-OPF problem, enabling the determination of missing reliability data to align with observed supply continuity levels. We apply this method to the real-world transmission network of Chile, solving various stochastic optimization problems, including the probabilistic transmission expansion planning problem. We showcase advanced techniques such as machine learning, decomposition, and regularization to effectively manage large-scale instances.

Our results significantly influenced the development of Chile's transmission network reliability standards in two chief ways. First, we demonstrated, from a pure cost-benefit analysis perspective, that further network investments were necessary and beneficial. We identified specific investments totalizing \$24.2 million per year in annuitized value, which would reduce expected energy not supplied cost by \$97.5 million per year, resulting in a net benefit of \$73.3 million per year for the consumers of the entire national power system. Secondly, we showed that the costs of meeting certain policy targets were disproportionate to their benefits. Instead, we proposed adopting a 3-hour SAIDI target per node, which was incorporated into the new network security standard enacted by NEC in 2020 [53].

Importantly, the Chilean case study presented in this paper constitutes a retrospective validation of the proposed methodology. The models developed in this work were provided to NEC staff during the formulation of the 2020 transmission network reliability standard, and NEC significantly contributed to the results presented in this paper. The regulatory process also involved roundtable discussions among academia, government, and industry, where the proposed models played a critical role in evaluating alternative hypotheses, informing the technical debate, and ultimately shaping the final reliability standards.

Finally, although the economic results reported in this work correspond to the regulatory context in which the study was originally conducted, the proposed inverse-calibration and reliability-oriented planning framework is independent of the particular technical, operational, and economic input data employed. Consequently, future applications can readily incorporate updated system data to reflect contemporary planning conditions without requiring any modification to the mathematical formulation of the proposed methodology.

APPENDIX PSC-OPF

This model corresponds to a PSC-OPF formulation that incorporates two post-contingency snapshots: a short-term one, in which generation units can only dispatch previously determined reserves as corrective actions and safe transfer limits are enforced, and a medium-term one, in which no reserve requirements or safe transfer limit constraints are imposed, allowing full reallocation of running generators. The objective function balances the costs and benefits of preventive and corrective actions by quantifying the cost of unsupplied demand through a load disconnection variable in both snapshots, further imposing that unsupplied demand in the medium-term snapshot does not exceed that of the short-term one, reflecting the greater operational flexibility available at that stage. Finally, to model reality more reliably, line losses are incorporated. All parameters, decision variables and the mathematical formulation of the PSC-OPF are presented below:

Sets and indices

Y	Set of all snapshots y, where $y = 1, 2$ represent the short- and medium-term post-contingency snapshots, and $y = 0$ is a pre-contingency snapshot used only for compact notation.
$\mathcal{A}$	Set of all index pairs (s, y) excluding the mixed pre/post combinations: $(s = 0 \wedge y > 0)$ and $(s > 0 \wedge y = 0)$.
L	Set of all assets of system S (transmission lines and transformers).
N	Set of all nodes n of the system.
S	Set of all contingency scenarios s, including the pre-contingency state $(s = 0)$.
G	Set of all generation units g of the system.
Z	Set of all geographical zones z into which the system is divided.
G_n	Set of all generation units g installed at node n.
G_z	Set of all generation units installed in geographical zone z.
ST	Set of all secure asset groups st sharing the same transfer limit.

Parameters

VoLL	Cost of energy not supplied [\$/MWh].
β_y	Weight for snapshot y.
$P(\hat{s})$	Probability of occurrence of contingency s (defined in Section IV).
$\hat{a}_{l,s}$	Indicator of failed asset l in scenario s (1 if failed; 0 otherwise).
$\mathrm{to}(l)$	Node n towards which line l enters.
$\mathrm{fr}(l)$	Node n from which line l exits.
M	Very large constant used for angular decoupling of failed assets.
F_l	Thermal limit for line l [MW].
$P_g^{\max}$, $P_g^{\min}$	Maximum and minimum generation limits for unit g [MW].
$r_g^{up,\max}$, $r_g^{down,\max}$	Maximum and minimum reserve limits for unit g [MW].
LST_{st}	Safe transfer limit for the secure asset group st.
R_z^{up}, R_z^{down}	Minimum reserve limits up and down for area z [MW].

D_n	Power demand at node n [MW].
FC_g	Capacity factor of generation unit g.
FP	Loss factor over the network (percentage of installed system capacity).
x_l	Reactance of line l [ohm].
length(l)	Length of line l.
u	Minimum length threshold [km] for an asset l to present losses.
CV_g	Variable cost of generation unit g [\$/MWh].
CR_g^{up}, CR_g^{down}	Cost of maintaining reserves up and down for unit g [\$/MWh].

Decision variables

$L_{n,s,y}$	Load shedding at node n of scenario s in snapshot y [MW].
$p_{g,0,0}$	Power generated for unit g in the pre-contingency state [MW].
$f_{l,0,0}$	Power flow through line l in the pre-contingency state [MW].
$f_{l,0,0}^{\text{pos}}$, $f_{l,0,0}^{\text{neg}}$	Power flows through line l in the pre-contingency state [MW], used to define losses.
$\theta_{n,0,0}$	Phase angle for node n in the pre-contingency state [rad].
$r_{g,0,0}^{up}$, $r_{g,0,0}^{down}$	Up and down reserves for unit g in the pre-contingency state [MW].
$x_{g,0,0} \in \{0, 1\}$	On/off commitment of generation unit g.
$p_{g,s,y}$	Power generated for unit g in scenario s of snapshot y under post-contingency conditions [MW].
$f_{l,s,y}$	Power flow through line l in scenario s of snapshot y under post-contingency conditions [MW].
$f_{l,s,y}^{\text{pos}}$, $f_{l,s,y}^{\text{neg}}$	Power flows through line l in scenario s of snapshot y under post-contingency conditions [MW], used to define losses.
$\theta_{n,s,y}$	Phase angle for node n in scenario s of snapshot y under post-contingency conditions [rad].

Mathematical formulation

$$\min \sum_{s\in S} P(\hat{s}) \cdot \sum_{y\in Y} \beta_y \cdot \Bigg[\sum_{g\in G} (\mathrm{CV}_{g,s,y} \cdot p_{g,s,y} + \mathrm{CR}_g^{up} \cdot r_{g,s,y}^{up} + \mathrm{CR}_g^{down} \cdot r_{g,s,y}^{down}) + \sum_{n\in N} \mathrm{VoLL} \cdot L_{n,s,y} \Bigg] \tag{A.1}$$

$$\sum_{g\in G_n} p_{g,s} + \sum_{l\in L:\, to(l)=n} f_{l,s} = D_n + \sum_{l\in L:\, fr(l)=n} f_{l,s} - L_{n,s,y} + \frac{1}{2} \sum_{\substack{l\in L: \\ (to(l)=n \vee fr(l)=n) \\ \text{length}(l)\geq u}} FP \cdot (f_{l,s,y}^{\text{pos}} + f_{l,s,y}^{\text{neg}})$$
$$\forall n \in N,\ \forall s \in S,\ \forall y \in Y,\ \text{with } (s, y) \in A \tag{A.2}$$

$$-M \cdot \hat{a}_{l,s} + \frac{1}{x_l} \cdot (\theta_{fr(l),s,y} - \theta_{to(l),s,y}) \leq f_{l,s,y} f_{l,s,y} \leq \frac{1}{x_l} \cdot (\theta_{fr(l),s,y} - \theta_{to(l),s,y}) + M \cdot \hat{a}_{l,s}$$
$$\forall n \in N,\ \forall s \in S,\ \forall y \in Y,\ \text{with } (s, y) \in A \tag{A.3}$$

$$f_{l,s,y} = f_{l,s,y}^{\text{pos}} - f_{l,s,y}^{\text{neg}}, \qquad \mathrm{SOS1}(f_{l,s,y}^{\text{pos}}, f_{l,s,y}^{\text{neg}})$$
$$\forall l \in L,\ \forall s \in S,\ \forall y \in Y,\ \text{with } (s, y) \in A \tag{A.4}$$

$$-(1 - \hat{a}_{l,s}) \cdot \overline{F}_l \leq f_{l,s,y} \leq \overline{F}_l \cdot (1 - \hat{a}_{l,s})$$
$$\forall l \in L,\ \forall s \in S,\ \forall y \in Y,\ \text{with } (s, y) \in A \tag{A.5}$$

$$-\,\mathrm{LST}_{st} \leq \sum_{l\in st} f_{l,0,0} \leq \mathrm{LST}_{st}\ \forall st \in \mathrm{ST} \tag{A.6}$$

$$p_{g,0,0} - r_{g,0,0}^{down} \leq p_{g,s,y} \leq p_{g,0,0} + r_{g,0,0}^{up},\quad \forall g \in G,\quad \forall s \in S\backslash\{0\},\quad \forall y \in Y\backslash\{2\},\ \text{with } (s, y) \in A \tag{A.7}$$

$$0 \leq L_{n,s,y} \leq D_n,\quad \forall n \in N,\ \forall s \in S,\quad \forall y \in Y\backslash\{2\},\ \text{with } (s, y) \in A \tag{A.8}$$

$$0 \leq L_{n,s,y} \leq L_{n,s,1},\quad \forall n \in N,\ \forall s \in S\backslash\{0\},\quad \forall y \in Y\backslash\{1\},\ \text{with } (s, y) \in A \tag{A.9}$$

$$p_{g,0,0} + r_{g,0,0}^{up} \leq P_g^{\max} \cdot x_{g,0,0} \cdot \mathrm{FC}_g \quad \forall g \in G \tag{A.10}$$

$$p_{g,0,0} - r_{g,0,0}^{down} \geq P_g^{\min} \cdot x_{g,0,0} \quad \forall g \in G \tag{A.11}$$

$$0 \leq r_{g,0,0}^{up} \leq r_g^{up,\max} \quad \forall g \in G \tag{A.12}$$

$$0 \leq r_{g,0,0}^{down} \leq r_g^{down,\max} \quad \forall g \in G \tag{A.13}$$

$$\sum_{g\in G_z} r_{g,0,0}^{up} \geq R_z^{up} \quad \forall z \in Z \tag{A.14}$$

$$\sum_{g\in G_z} r_{g,0,0}^{down} \geq R_z^{down} \quad \forall z \in Z \tag{A.15}$$

$$P_g^{\min} \cdot x_{g,s,y} \leq p_{g,s,y} \leq P_g^{\max} \cdot x_{g,s,y} \cdot \mathrm{FC}_g,\quad \forall g \in G,\ \forall s \in S\backslash\{0\},\quad \forall y \in Y\backslash\{1\},\ \text{with } (s, y) \in A \tag{A.16}$$

$$L_{n,0,0} = 0, \quad \forall n \in N \tag{A.17}$$

$$r_{g,s,y}^{up} = 0, \quad \forall g \in G,\ \forall s \in S\backslash\{0\},\ \forall y \in Y\backslash\{0\} \tag{A.18}$$

$$r_{g,s,y}^{down} = 0, \quad \forall g \in G,\ \forall s \in S\backslash\{0\},\ \forall y \in Y\backslash\{0\} \tag{A.19}$$

$$x_{g,s,y} \in \{0, 1\},$$
$$\forall g \in G,\ \forall s \in S,$$
$$\forall y \in Y \backslash \{1\},\ \text{with } (s, y) \in A \tag{A.20}$$

where (A.1) represents the objective function to be minimized, which is weighted by the probability of contingencies, and considers the pre-contingency state operating costs plus the cost of corrective actions of the short (reserve dispatch) and medium term (generation unit reallocation) weighted post-contingency snapshot, (A.2) represents the nodal balancing constraint with load shedding, (A.3)-(A.5) represent the angular coupling (A.3), the losses (A.4), and the thermal limits on the transmission lines (A.5), for all contingency scenarios including the pre-contingency state, (A.6) represents the safe transfer limits for transmission lines in the pre-contingency state, (A.7) represents the corrective action constraints, (A.8) represents the maximum allowed load shedding limit, (A.9) models the fact that the increased flexibility in the medium-term snapshot causes the load shedding to be lower than that obtained in the short-term snapshot, (A.10)-(A.15) model the generation and reserve limit constraints for the pre-contingency state, (A.16) model the generation limit constraints for middle-term snapshot, (A.17)-(A.19) represent consistency constraints due to the use of compact notation, and (A.20) sets as binary variables the switching on and off of generation units.

REFERENCES

[1] P. Joskow, "Patterns of transmission investments," in *Competitive Electricity Markets and Sustainability*. François Lévêque, Cheltenham, U.K.: Edward Elgar Publishing, 2006.

[2] G. Strbac, D. Kirschen, and R. Moreno, "Reliability standards for the operation and planning of future electricity networks," *Found. Trends Electric Energy Syst.*, vol. 1, no. 3, pp. 143–219, Dec. 2016.

[3] U. Shahzad, "Probabilistic security assessment in power transmission systems: A review," *J. Elect. Eng., Electron., Control Comput. Sci.*, vol. 7, no. 4, pp. 25–32, 2021.

[4] M. Vrakopoulou, S. Chatzivasileiadis, E. Iggland, M. Imhof, T. Krause, O. Mäkelä, J. L. Mathieu, L. Roald, R. Wiget, and G. Andersson, "A unified analysis of security-constrained OPF formulations considering uncertainty, risk, and controllability in single and multi-area systems," in *Proc. IREP Symp. Bulk Power Syst. Dyn. Control IX Optim., Secur. Control Emerg. Power Grid*, Aug. 2013, pp. 1–19.

[5] A. B. Rodrigues and M. d. G. da Silva, "Confidence intervals estimation for reliability data of power distribution equipments using bootstrap," *IEEE Trans. Power Syst.*, vol. 28, no. 3, pp. 3283–3291, Aug. 2013.

[6] D. Alvarado, R. Moreno, M. E. Orchard, and D. S. Kirschen, "Cost-benefit analysis of maintenance plans: Case study of the power system of a large industrial facility," *IEEE Trans. Power Syst.*, vol. 38, no. 3, pp. 2046–2057, May 2023.

[7] T. C. Y. Chan, R. Mahmood, and I. Y. Zhu, "Inverse optimization: Theory and applications," *Oper. Res.*, vol. 73, no. 2, 2025.

[8] B. Hu, K. Xie, and H.-M. Tai, "Inverse problem of power system reliability evaluation: Analytical model and solution method," *IEEE Trans. Power Syst.*, vol. 33, no. 6, pp. 6569–6578, Nov. 2018.

[9] T. Niu, F. Li, B. Hu, H. Lu, L. Peng, K. Xie, K. Cao, and K. Zhou, "Research on the inverse problem of reliability evaluation–model and algorithm," *IEEE Access*, vol. 9, pp. 12648–12656, 2021.

[10] S. Sharifinia, M. Rastegar, M. Allahbakhshi, and M. Fotuhi-Firuzabad, "Inverse reliability evaluation in power distribution systems," *IEEE Trans. Power Syst.*, vol. 35, no. 1, pp. 818–820, Jan. 2020, doi: 10.1109/TPWRS.2019.2952518.

[11] F. Capitanescu, M. Glavic, D. Ernst, and L. Wehenkel, "Applications of security-constrained optimal power flows," in *Proc. Mod. Electr. Power Systems Symp. (MEPS)*, Wroclaw, Poland, 2006.

[12] F. Capitanescu, J. L. M. Ramos, P. Panciatici, D. Kirschen, A. M. Marcolini, L. Platbrood, and L. Wehenkel, "State-of-the-art, challenges, and future trends in security constrained optimal power flow," *Electr. Power Syst. Res.*, vol. 81, no. 8, pp. 1731–1741, Aug. 2011.

[13] K. Beven and J. Freer, "Equifinality, data assimilation, and uncertainty estimation in mechanistic modelling of complex environmental systems using the GLUE methodology," *J. Hydrol.*, vol. 249, nos. 1–4, pp. 11–29, Aug. 2001.

[14] K. Beven, "A manifesto for the equifinality thesis," *J. Hydrol.*, vol. 320, nos. 1–2, pp. 18–36, Mar. 2006.

[15] K. Kariuki and R. Allan, "Applications of customer outage costs in system planning, design and operation," *IEE Proc. Gener., Transmiss. Distrib.*, vol. 143, no. 4, pp. 305–312, 1996.

[16] D. Alvarado, A. Moreira, R. Moreno, and G. Strbac, "Transmission network investment with distributed energy resources and distributionally robust security," *IEEE Trans. Power Syst.*, vol. 34, no. 6, pp. 5157–5168, Nov. 2019.

[17] M. Rios, D. Kirschen, D. Jayaweera, D. Nedic, and R. Allan, "Value of security: Modeling time dependent phenomena and weather conditions," *IEEE Trans. Power Syst.*, vol. 17, pp. 543–548, 2002.

[18] M. Bhuiyan and R. Allan, "Inclusion of weather effects in composite system reliability evaluation using sequential simulation," *IEE Proc. Gener., Transmiss. Distrib.*, vol. 141, no. 6, pp. 1359–7051, 1994.

[19] R. Billinton and R. N. Allan, *Reliability Evaluation of Power Systems*. Cham, Switzerland: Springer, 1996.

[20] W. Li, *Risk Assessment of Power Systems: Models, Methods, and Application*. Hoboken, NJ, USA: Wiley, 2014.

[21] R. E. Brown and M. Marshall, "Budget constrained planning to optimize power system reliability," *IEEE Trans. Power Syst.*, vol. 15, no. 2, pp. 887–892, May 2000.

[22] R. N. Allan, R. Billinton, I. Sjarief, L. Goel, and K. S. So, "A reliability test system for educational purposes-basic distribution system data and results," *IEEE Trans. Power Syst.*, vol. 6, no. 2, pp. 813–820, May 1991.

[23] R. M. Bucci, R. V. Rebbapragada, A. J. McElroy, E. A. Chebil, and S. Driller, "Failure prediction of underground distribution feeder cables," *IEEE Trans. Power Del.*, vol. 9, no. 4, pp. 1943–1955, 1994.

[24] D. T. Radmer, P. A. Kuntz, R. D. Christie, S. S. Venkata, and R. H. Fletcher, "Predicting vegetation-related failure rates for overhead distribution feeders," *IEEE Trans. Power Del.*, vol. 17, no. 4, pp. 1170–1175, Oct. 2002.

[25] S. Gupta, A. Pahwa, Y. Zhou, S. Das, and R. E. Brown, "An adaptive fuzzy model for failure rates of overhead distribution feeders," *Electr. Power Compon. Syst.*, vol. 33, no. 11, pp. 1175–1190, Nov. 2005.

[26] W. Wang, M. Wang, X. Han, M. Yang, Q. Wu, and R. Li, "Distributionally robust transmission expansion planning considering uncertainty of contingency probability," *J. Modern Power Syst. Clean Energy*, vol. 10, no. 4, pp. 894–901, Jul. 2022.

[27] R. E. Brown and J. R. Ochoa, "Distribution system reliability: Default data and model validation," *IEEE Trans. Power Syst.*, vol. 13, no. 2, pp. 704–709, May 1998.

[28] R. E. Brown, G. Frimpong, and H. L. Willis, "Failure rate modeling using equipment inspection data," *IEEE Trans. Power Syst.*, vol. 19, no. 2, pp. 782–787, May 2004.

[29] B. Canizes, J. Soares, Z. Vale, and C. Lobo, "Optimal approach for reliability assessment in radial distribution networks," *IEEE Syst. J.*, vol. 11, no. 3, pp. 1846–1856, Sep. 2017.

[30] A. Sallam, M. Desouky, and H. Desouky, "Evaluation of optimal-reliability indices for electrical distribution systems," *IEEE Trans. Rel.*, vol. 39, no. 3, pp. 259–264, Aug. 1990.

[31] C.-T. Su and G.-R. Lii, "Reliability design of distribution systems using modified genetic algorithms," *Electric Power Syst. Res.*, vol. 60, no. 3, pp. 201–206, Jan. 2002.

[32] W.-F. Chang and Y.-C. Wu, "Optimal reliability design in an electrical distribution system via a polynomial-time algorithm," *Int. J. Electr. Power Energy Syst.*, vol. 25, no. 8, pp. 659–666, Oct. 2003.

[33] L. D. Arya, S. C. Choube, and R. Arya, "Differential evolution applied for reliability optimization of radial distribution systems," *Int. J. Electr. Power Energy Syst.*, vol. 33, no. 2, pp. 271–277, Feb. 2011.

[34] C.-T. Su and G.-R. Lii, "Reliability planning for composite electric power systems," *Electr. Power Syst. Res.*, vol. 51, no. 1, pp. 23–31, Jul. 1999.

[35] R. A. Bakkiyaraj and N. Kumarappan, "Optimal reliability planning for a composite electric power system based on Monte Carlo simulation using particle swarm optimization," *Int. J. Electr. Power Energy Syst.*, vol. 47, pp. 109–116, May 2013.

[36] K. Xie, R. Billinton, and J. Zhou, "Tracing the unreliability contributions of power system components," *Electr. Power Compon. Syst.*, vol. 36, no. 12, pp. 1299–1309, Nov. 2008.

[37] K. Xie and R. Billinton, "Tracing the unreliability and recognizing the major unreliability contribution of network components," *Rel. Eng. Syst. Saf.*, vol. 94, no. 5, pp. 927–931, May 2009.

[38] K. Xie, B. Hu, and R. Karki, "Tracing the component unreliability contributions and recognizing the weak parts of a bulk power system," *Eur. Trans. Electr. Power*, vol. 21, no. 1, pp. 254–262, Jan. 2011.

[39] A. Monticelli, M. V. F. Pereira, and S. Granville, "Security-constrained optimal power flow with post-contingency corrective rescheduling," *IEEE Trans. Power Syst.*, vol. PS-2, no. 1, pp. 175–180, Feb. 1987.

[40] R. Billington and R. N. Allan, *Reliability Evaluation of Power Systems*. New York, NY, USA: Plenum Press, 1984.

[41] V. Krishnan, J. Ho, B. F. Hobbs, A. L. Liu, J. D. McCalley, M. Shahidehpour, and Q. P. Zheng, "Co-optimization of electricity transmission and generation resources for planning and policy analysis: Review of concepts and modeling approaches," *Energy Syst.*, vol. 7, no. 2, pp. 297–332, May 2016.

[42] H. Zhang, V. Vittal, G. T. Heydt, and J. Quintero, "A mixed-integer linear programming approach for multi-stage security-constrained transmission expansion planning," *IEEE Trans. Power Syst.*, vol. 27, no. 2, pp. 1125–1133, May 2012.

[43] R. Moreno, D. Pudjianto, and G. Strbac, "Transmission network investment with probabilistic security and corrective control," *IEEE Trans. Power Syst.*, vol. 28, no. 4, pp. 3935–3944, Nov. 2013.

[44] T. Asamov and W. B. Powell, "Regularized decomposition of high-dimensional multistage stochastic programs with Markov uncertainty," *SIAM J. Optim.*, vol. 28, no. 1, pp. 575–595, Jan. 2018.

[45] F. Cordera, R. Moreno, and F. Ordoñez, "Unit commitment problem with energy storage under correlated renewables uncertainty," *Oper. Res.*, vol. 71, no. 6, pp. 1960–1977, Nov. 2023.

[46] *Energia 2050 Politica Energetica de Chile*, Ministerio de Energía, Santiago, Chile, 2015.

[47] *Documentos de Modelacion del SEN*, Coordinador Eléctrico Nacional, Santiago, Chile, 2019.

[48] *Decreto 6 T*, Ministerio de Energía, Santiago, Chile, 2017.

[49] *Resolucion Exenta 227*, Ministerio de Energía, Santiago, Chile, 2018.

[50] *Informe Definitivo Estudio de Continuidad de Suministro*, Coordinador Eléctrico Nacional, Santiago, Chile, 2018.

[51] *Estudio de Restricciones en el Sistema de Transmision*, Coordinador Eléctrico Nacional, Santiago, Chile, 2018.

[52] J. Zhang and A. Sanderson, *Adaptive Differential Evolution: A Robust Approach to Multimodal Problem Optimization*. Cham, Switzerland: Springer, 2009.

[53] *Norma Tecnica de Indisponibilidad de Suministro y Compensaciones*, Comisión Nacional de Energía, Santiago, Chile, 2020.

FELIPE SEPÚLVEDA received the B.Sc. degree in industrial engineering from the University of Concepción, Concepción, Chile, and the M.Sc. degree in operations research from the University of Chile, Santiago, Chile, where he is currently pursuing the Ph.D. degree in complex engineering systems. His research interests include power systems economics, operation, and planning.

DIEGO ALVARADO received the B.Sc. and M.Sc. degrees in electrical engineering from the University of Chile, Santiago, Chile. He currently works in the electric power industry. His research interests include power systems economics, operation, and planning.

FELIPE CORDERA is currently pursuing the Ph.D. degree with the Operations Research Center, Massachusetts Institute of Technology. His research interests include applying mathematical programming techniques to solve complex optimization problems, particularly those affected by uncertainty and high dimensionality, with a keen interest in decomposition methods and modeling aspects.

EDUARDO ESPERGUEL received the B.Sc. degree in electrical civil engineering from the University of Chile, Santiago, Chile. He has 15 years of professional experience in power transmission and electricity sector regulation, including roles as the Head of the Transmission Planning Sub Department and the Acting Head of the Electricity Department, Chilean National Energy Commission. His research interests include transmission expansion planning, power system regulation, and electricity market design.

GORAN STRBAC (Fellow, IEEE) is currently a Professor in electrical energy systems with Imperial College, London, U.K. His research interests include electricity generation, transmission and distribution operation, planning and pricing, and the integration of renewable and distributed generation in electricity systems.

RODRIGO MORENO (Member, IEEE) received the B.Sc. and M.Sc. degrees from the Pontificia Universidad Católica de Chile, Santiago, Chile, and the Ph.D. degree from Imperial College London, London, U.K. He is currently the Director of the Energy Engineering Program at the Faculty of Engineering and Sciences, Universidad Adolfo Ibáñez, Santiago, Chile. His research interests include power system optimization, reliability and economics, renewable energy, and smart grids.